Turk J Agric For
31 (2007) 135-145

Relationships between Remotely Sensed Data and Biomass Components in a Big Sagebrush (*Artemisia tridentata*) Dominated Area in Yellowstone National Park

Mustafa MİRİK[1,*], Jack E. NORLAND[2], Mario E. BIONDINI[2], Robert L. CRABTREE[3], Gerald J. MICHELS, Jr.[1]

[1]The Texas A&M University System, Agricultural Research and Extension Center,

6500 Amarillo Boulevard West, Amarillo, TX 79106, USA.

[2]North Dakota State University, Hultz Hall, Fargo, ND 58105 - USA.

[3]The Yellowstone Ecological Research Center, 2048 Analysis Drive, Suite B, Bozeman, MT 59715 - USA.

Received: 06.09.2006

Abstract: The predictive power of a hyperspectral imagery for estimating woody and herbaceous biomass were examined for a big sagebrush (*Artemisia tridentata*) dominated area in Yellowstone National Park, Wyoming, United States of America. The normalized difference vegetation (NDV) and structure insensitive pigment (SIP) indices were used to investigate the relationships between biomass components and reflectance spectra. Ground data were collected in 13 sample plots 1 m^2 in size by clipping all herbaceous vegetation to ground level and stripping green leaves from big sagebrush plants. Strong relationships (R^2 from 0.83 to 0.96) were found between the hyperspectral data and biomass components. The results indicate that fine resolution hyperspectral imagery is capable of estimating various biomass components in big sagebrush dominated areas.

Key Words: Hyperspectral imagery, indices, big sagebrush, biomass, Yellowstone National Park

Yellowstone Milli Park'ındaki Büyük Sage Çalısı (*Artemisia tridentata*) Alanındaki Biyomas Bileşenleri ve Uzaktan algılanmış Veriler Arasındaki İlişkiler

Özet: Bu araştırma yüksek yersel ve tayf çözünürlüğüne sahip bir hava görüntüsünün Amerika Birleşik Devletleri, Wyoming eyaletindeki Yellowstone Milli Parkındaki büyük sage çalısı (*Artemisia tridentata*) alanındaki biyoması tahmin etme gücü üzerine yapılmıştır. Biyomas ile yansıtma değerleri arasındaki ilişkiyi incelemek amacıyla farkları normalleştirilmiş bitki (NDV) ve yapısal bağımsız pigment (SIP) indisleri kullanılmıştır. Arazideki bitki kütlesi 13 tane bir metre karelik alanlarda bütün otsu bitkilerin toprak yüzeyinden kesilmesi ve büyük sage çalısı yapraklarının elle sıyrılarak toplanması şeklinde gerçekleştirilmiştir. Biyomass bileşenleri ve yüksek çözünürlüklü hava verileri arasında güçlü bir ilişki bulunmuştur (R^2 = 0.83-0.96). Elde edilen sonuçlar yüksek tayf ve yersel çözünürlüğe sahip olan hyperspektral uzaktan algılama verilerinin büyük sage çalısı alanlarındaki biyomas tahminine elverişli olduğunu göstermiştir.

Anahtar Sözcükler: Hava görüntüsü, indisler, büyük sage çalısı, biyomas, Yellowstone Milli Parkı

Introduction

Remote sensing has been argued to have advantages over traditional ground-based monitoring methods, because the latter are laborious, slow, limited to the localized areas, subject to great variation, and constrained by the lack of access (Bork et al., 1999; Gemmell and Varjo, 1999). Some of the latest studies have shown that one of the most important and promising uses of remote sensing is to determine cover, leaf area index, and seasonal dynamics of sparse vegetation in arid and semiarid environments (Jakubauskas et al., 2001; Okin et al., 2001). Remote sensing studies of sagebrush steppes are of great interest because of the vast areas covered by woody sagebrush communities in western North America.

*Correspondence to: mustafamirik@gmail.com

Sagebrush species occupy about 1,087,795 km^2 in 11 western states (Beetle and Johnson, 1982). The most common and abundant single sagebrush species is big sagebrush (*Artemisia tridentata*), found from southern Canada to northern Mexico (Beetle and Johnson, 1982; McArthur and Welch, 1982). Big sagebrush and its associated plant communities are an essential component of ecosystem structure and functioning, and are critically important for livestock production, watershed management, and wildlife such as the potentially endangered greater sage-grouse (*Centrocercus urophasianus*).

The monitoring of the quantity and dynamics of both green and woody biomass of big sagebrush is important, but only a limited number of previous studies using remote sensing technology have focused on sagebrush areas (Jakubauskas et al., 2001; Ramsey et al., 2004). The objective of this study was to quantify the relationship between big sagebrush woody and herbaceous biomass and spectral vegetation indices. The second objective was to simulate bands of Enhanced Thematic Mapper Plus (ETM+) and Le Systeme Pour l'Observation de la Terre-5 (SPOT-5) from the hyperspectral imagery in order to compare the predictive power of multispectral and hyperspectral data.

Materials and Methods

Study site

The study site was located on the northern winter range at the confluence of the Lamar River and Soda Butte Creek (Figure 1) in Yellowstone National Park. Yellowstone National Park covers about 899,500 ha between 44º08´ and 45º07´ N, and 111º10´ and 110º W in the northwestern corner of Wyoming. The vegetation of the study region is a mixture of steppe, shrub-steppe, forest, and riparian areas. Grassland and sagebrush/Idaho fescue (*Artemisia tridentata/Festuca idahoensis*) habitat types occur on 55% of the northern winter range of the park (Barmore, 1980). Big sagebrush (*Artemisia tridentata*) dominates the over-story in the sagebrush/Idaho fescue habitat type. The under-story is

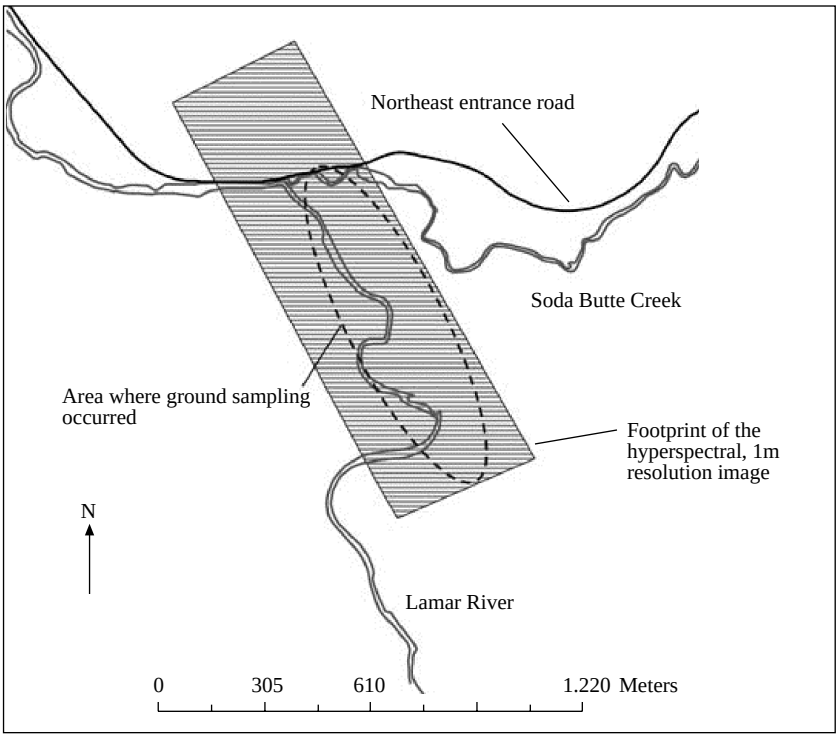

Figure 1. Map of the study site, location of the ground sample plots, and hyperspectral imagery footprint in the northeast corner of Yellowstone National Park, Wyoming, United States of America.

dominated by bluebunch wheatgrass (*Agropyron spicatum*), junegrass (*Koeleria macrantha*), Idaho fescue (*Festuca idahoensis*), needlegrasses (*Stipa comata*), basin wild rye (*Elymus cinereus*), bluegrasses (*Poa* spp.), and various forbs.

Ground data collection

The ground data sites were selected to represent a large range of biomass available in the big sagebrush dominated plant communities. A large range of values is needed to fully establish relationships between ground and hyperspectral data. Ground data sites were selected rather than randomly chosen because randomly selected sites might not have contained the full range of biomass values needed given the time and personnel constraints available for the study.

The sample locations were mapped directly to the imagery as is commonly done in air photos. Using the imagery like an air photo, landmarks such as the scattered individual trees were exactly matched to a pixel in the image. The sample locations were then selected and the distance and angle of the ground data sites to the landmarks were measured with a tape and compass, respectively. Using the distance and angle measurements in combination with the landmark pixel, a pixel in the image was identified that corresponded to the ground samples. This method, as found by Aspinall et al. (2002), produced matches between the pixel and the ground sample that were off by less than 1 m, whereas using a georeferenced image and GPS coordinates of the ground sites produced errors >2 m. The locations of the ground sites were far enough away from large objects to avoid the shadowing effects at the sites.

Ground data were collected from 13 quadrats 1 m^2 in size over the study site on August 7 and 8, 1999. Ground data were collected 5 days after the flight. A plot size of 1 m^2 was selected for ground data collection so as to match the spatial resolution of the PROBE-1 imagery. Grasses and forbs were clipped to ground level. Big sagebrush leaves (non-woody portion) were stripped by hand in the 1 m^2 plots. All vegetation was placed in paper bags and transported to the laboratory. Vegetation samples were weighed after oven drying at 60 ºC for at least 48 h. Dried and weighed samples were further categorized into sagebrush only green biomass (the hand-stripped leaves) (SB hereafter), total biomass including litter (TB hereafter), and total biomass without sagebrush only green biomass (TBWSB hereafter). TB contained sagebrush green leaf material, forbs, grass, and litter. TBWSB is equal to TB minus sagebrush green leaves (TBWSB = TB – SB). Pictures of the remaining woody parts of the big sagebrush were taken by a digital camera in order to develop a sagebrush woody vegetation index (WVI). Digital pictures were taken at a standard height directly above the plots. WVI was calculated by placing equal-sized grids on each of the digital pictures. The numbers of grid intersections that encountered the woody parts of the sagebrush were divided by the number of total grid intersections for the WVI calculation.

Spectral data collection

The remote sensing data was collected using the PROBE-1 hyperspectral system of Earth Search Science, Inc., McCall, ID, USA. The hyperspectral imagery was collected on August 2, 1999, at a spatial resolution of 1 m from an A-Star Aerospatiale helicopter flying approximately 600 m above the ground. The imagery consisted of 511 pixels wide and 1920 pixels long. Geometric correction of the imagery was done with an onboard Global Positioning System/Inertial Navigation System, C-MIGITS-II, and a ray-tracing technique. The PROBE-1 is a whiskbroom-style instrument that gathers information in a cross-track direction by mechanical scanning in an along-track direction by movement of the airborne platform. The PROBE-1 remote sensing detector collected reflectance data from about 423 to 2507 nm of the electromagnetic spectrum with average, minimum, and maximum bandwidths of 15, 10.7, and 19.8 nm, respectively. The detector consisted of 4 spectrographs, each of which had 32 bands, for a total of 128 bands. There were approximately 24 and 161 nm gaps between second and third and third and fourth spectrographs, respectively. The sensor has a signal-to-noise ratio around 1500:1 for the visible and NIR wavelengths and 800:1 for the Middle Infrared (MIR) (McGwire et al., 2000; ESSI, 2001). The hyperspectral data were not atmospherically corrected because the flight occurred at such low altitude that atmospheric distortions were minimized (Aspinall et al., 2002). Furthermore, because of the small extent of the image, atmospheric problems were not different across the image and thus whatever atmospheric distortion might have occurred was similar across pixels.

Analysis

Imagery analysis was conducted using the Environment for Visualizing Images (ENVI) software package (Research System Inc., Boulder, CO, USA). Values of pixels coupling with ground plots were extracted and transferred into Statistical Analysis System (SAS Institute, Inc., Cary, NC, USA) for statistical analysis. Initially, the relationships between 25 vegetation indices derived from the hyperspectral imagery and amount of vegetation biomass were investigated. Of these indices tested, the structure insensitive pigment index (SIPI) proposed by Peñuelas et al. (1995) and the normalized difference vegetation index (NDVI), probably the most popular index in the remote sensing community, developed by Rouse et al. (1973), had the highest correlations with woody and herbaceous biomass components. Based on these preliminary results, these 2 spectral vegetation indices were further modified. The approach exercised in this study to compute SIP and NDV indices was as follows:

Original formulae:

$$SIPI = \frac{(NIR_{800} - Blue_{445})}{(NIR_{800} - \mathrm{Red}_{680}} \quad (1)$$

$$NDVI = \frac{(NIR_{845} - \mathrm{Red}_{648})}{(NIR_{845} - \mathrm{Red}_{648}} \quad (2)$$

and modified versions

$$SIPI = \frac{(NIR_{19} - Blue_1)}{(NIR_{19} - \mathrm{Red}_{12})}, \frac{(NIR_{19} - Blue_2)}{(NIR_{19} - \mathrm{Red}_{12})} \ldots \frac{(NIR_{19} - Blue_{11})}{(NIR_{19} - \mathrm{Red}_{12})}$$

$$= \frac{(NIR_{19} - Blue_1)}{(NIR_{19} - \mathrm{Red}_{13})}, = \frac{(NIR_{19} - Blue_1)}{(NIR_{19} - \mathrm{Red}_{14})} \ldots = \frac{(NIR_{19} - Blue_1)}{(NIR_{19} - \mathrm{Red}_{18})},$$

$$= \frac{(NIR_{20} - Blue_1)}{(NIR_{20} - \mathrm{Red}_1)}, = \frac{(NIR_{21} - Blue_1)}{(NIR_{21} - \mathrm{Red}_1)}, \ldots, = \frac{(NIR_{128} - Blue_{11})}{(NIR_{128} - \mathrm{Red}_{18})} \quad (3)$$

where

Blue spectrum ranged from 438 to 586 nm with a total of 11 bands.

Red spectrum ranged from 601 to 693 nm with a total of 7 bands.

NIR spectrum ranged from 708 to 2507 nm with a total of 110 bands in SIPI.

$$NDVI = \frac{(NIR_{26} - \mathrm{Red}_1)}{(NIR_{26} + \mathrm{Red}_1)}, = \frac{(NIR_{26} - \mathrm{Red}_2)}{(NIR_{26} + \mathrm{Red}_2)}, \ldots,$$

$$= \frac{(NIR_{26} - \mathrm{Red}_{25})}{(NIR_{26} + \mathrm{Red}_{25})}, = \frac{(NIR_{27} - \mathrm{Red}_1)}{(NIR_{27} + \mathrm{Red}_1)},$$

$$= \frac{(NIR_{27} - \mathrm{Red}_2)}{(NIR_{27} + \mathrm{Red}_2)}, \ldots, = \frac{(NIR_{27} - \mathrm{Red}_{25})}{(NIR_{27} + \mathrm{Red}_{25})}, \ldots,$$

$$= \frac{(NIR_{128} - \mathrm{Red}_{25})}{(NIR_{128} + \mathrm{Red}_{25})} \quad (4)$$

where

Red spectrum ranged from 438 to 799 nm with a total of 25 bands.

NIR spectrum ranged from 814 to 2507 nm with a total of 103 bands in NDVI.

ETM+ and SPOT-5 bands were simulated by taking the average of the bands falling in the same regions of visible (blue, green, red), NIR, and Middle Infrared (MIR) of ETM+ and SPOT-5. Spatial and spectral specifications of ETM+ and SPOT-5 are presented in Table 1. The NDV and SIP indices were calculated with the following equations for these sensors.

$$NDVI = \frac{(Bi - Bj)}{(Bi + Bj)} \quad (5)$$

Bi = from green to MIR bands for ETM+ and from red to MID bands for SPOT-5.

Bj = from blue to Bi-1 bands for ETM+ and from green to Bi-1 bands for SPOT-5.

$$SIPI = \frac{(Bi - Bj)}{(Bi - Bk)} \quad (6)$$

Table 1. Spatial and spectral specifications of Enhanced Thematic Mapper Plus (ETM+) and Le Systeme Pour l'Observation de la Terre-5 (SPOT-5)

Enhanced Thematic Mapper Plus (ETM+)		
Band	Spectral resolution (μm)	Spatial resolution (m)
1 (blue)	0.45-0.52	30
2 (green)	0.52-0.60	30
3 (red)	0.63-0.69	30
4 (near infrared)	0.76-0.90	30
5 (middle infrared)	1.55-1.75	30
6 (thermal infrared)	10.40-12.50	60
7 (middle infrared)	2.08-2.35	30
8 (panchromatic)	0.52-0.90	15
Le Systeme Pour l'Observation de la Terre-5 (SPOT-5)		
1 (green)	0.50-0.59	10
2 (red)	0.61-0.68	10
3 (near infrared)	0.78-0.89	10
4 (middle infrared)	1.58-1.75	20
Panchromatic	0.48-0.71	2.5 or 5

Bi = from red to MID bands for ETM+ and NIR and MID bands for SPOT-5

Bj = from blue to Bk-1 bands for ETM+ and from green to Bk-1 bands for SPOT-5.

Bk = from green to Bi-1 bands for ETM+ and from red to Bi-1 bands for SPOT-5.

The PROC STEPWISE regression procedure of SAS was used and set to the MAXR model-selection method. The MAXR model-selection method identifies the best single and multiple regression models depending on the user choice, with the highest R^2. A weighting procedure in regression analysis was performed. Weighting in least-square regression corrects the problem of heteroskedasticity by log-likelihood estimation of a weight that adjusts the errors of prediction. Namely, this method can sometimes improve the fit of regression models with repeated values in the predictor. Therefore, weighted regression is an appropriate method in those situations where it is known a priori that not all observations contribute equally to the fit (S-PLUS 2001; Insightful Inc, Seattle, WA, USA). Data were also transformed to the logarithm, square, and inversion of the variables to see whether prediction improved or not. In transformed data, for example logarithmic transformation, the larger values are squeezed together and smaller values are stretched out in order to correct skewed data, outliers, and unequal variation (Simon, 2006). Biomass components were set as the dependent variables and vegetation indices were set as the independent variables.

Results and Discussion

The descriptive statistics for biomass components are presented in Table 2. The mean for TB, SB, TBWSB, and WVI was 170, 68, 101 g m^{-2}, and 23, respectively. The relationships between vegetation indices and biomass component varied widely. The Probe-1-derived NDVI produced better relationships with only TB and TBWSB when compared with the SIPI. The SIPI calculated for the ETM+ and SPOT-5 exhibited the highest coefficients of determination (R^2) for all biomass components. The relationships between vegetation indices and biomass components were greatly improved by transforming and weighing the data (Tables 3-6).

Total biomass (TB)

Vegetation indices, procedures applied to the original data, and R^2 and probability (P) values for each of the 3

Table 2. Summary statistics of biomass components taken in 13, 1 m^2 sample plots in Yellowstone National Park, Wyoming, United States of America, on August 7-8, 1999.

Biomass Components	Max.	Mean.	Min.	Std. Dev.	UCL (0.95)	LCL (0.95)
TB (g m^{-2})	273	170	80	72	213	126
SB (g m^{-2})	183	68	20	54	101	36
TBWSA (g m^{-2})	167	101	34	48	130	72
WVI	65	23	5	18	34	13

Max.: Maximum, Min.: Minimum, Std. Dev.: Standard Deviation, UCL: Upper confidence limit, LCL: Lower confidence limit, TB: Total biomass, SB: Sagebrush only green biomass, TBWSB: Total biomass without sagebrush only green biomass, WVI: Woody vegetation index.

Table 3. Coefficients of determination (R^2) associated with vegetation indices and total biomass (TB) collected in Yellowstone National Park, Wyoming, United States of America, on August 7-8, 1999.

Instrument	Index	Index Formula	Biomass Component	R^2	P
Probe-1	SIPI	$(R_{800}-R_{449})/(R_{800}-R_{678})$	TB	0.32	0.04
Probe-1	NDVI	$(R_{845}-R_{648})/(R_{845}+R_{648})$	TB	0.31	0.04
Probe-1	MNDVI	$(R_{896}-R_{724})/(R_{896}+R_{724})$	TB	0.75	< 0.01
Probe-1	$MNDVI^2$	$(R_{896}-R_{724})/(R_{896}+R_{724})^2$	1/TB	0.83	< 0.01
ETM+	SIPI	$(B_{NIR}-B_{BLUE})/(B_{NIR}-B_{RED})$	TB	0.41	0.01
ETM+	NDVI	$(B_{NIR}-B_{RED})/(B_{NIR}+B_{RED})$	TB	0.33	0.04
ETM+	$SIPI^2$	$(B_{NIR}-B_{BLUE})/(B_{NIR}-B_{RED})^2$	$1/TB_w$	0.55	< 0.01
SPOT-5	SIPI	$(B_{NIR}-B_{GREEN})/(B_{NIR}-B_{RED})$	TB	0.60	< 0.01
SPOT-5	NDVI	$(B_{NIR}-B_{RED})/(B_{NIR}+B_{RED})$	TB	0.33	0.04
SPOT-5	$SIPI^2_w$	$(B_{NIR}-B_{GREEN})/(B_{NIR}-B_{RED})^2_w$	1/TB	0.84	< 0.01

P: Probability value for the regression model; SIPI: Structure insensitive pigment index; R_{800} and R_{449}: Reflectance values of wavebands centered at 800 and 449 nm of the electromagnetic spectrum; NDVI: Normalized difference vegetation index; MNDVI: Modified NDVI; ETM+: Enhanced Thematic Mapper Plus; SPOT-5: Le System Pour l'Observation de la Terre-5; B_{NIR} and B_{BLUE}: Near infrared and blue bands of ETM+ and SPOT-5, 1/TB: Inversion of TB; $_w$: weighted variable.

Table 4. Coefficients of determination (R^2) associated with vegetation indices and sagebrush only green biomass (SB) collected in Yellowstone National Park, Wyoming, United States of America, on August 7-8, 1999.

Instrument	Index	Index Formula		Variable	R^2P
Probe-1	SIPI	$(R_{800}-R_{449})/(R_{800}-R_{678})$	SB	0.05	0.78
Probe-1	NDVI	$(R_{845}-R_{648})/(R_{845}+R_{648})$	SB	0.05	0.79
Probe-1	MSIPI	$(R_{944}-R_{438})/(R_{944}-R_{678})$	SB	0.79	< 0.01
Probe-1	$MSIPI^2$	$(R_{944}-R_{438})/(R_{944}-R_{678})^2$	SB_w	0.93	< 0.01
ETM+	SIPI	$(B_{NIR}-B_{BLUE})/(B_{NIR}-B_{RED})$	SB	0.05	0.45
ETM+	NDVI	$(B_{NIR}-B_{RED})/(B_{NIR}+B_{RED})$	SB	0.01	0.80
ETM+	MSIPI	$(B_{NIR}-B_{BLUE})/(B_{NIR}-B_{GREEN})$	SB	0.07	0.38
ETM+	$MSIPI^2_w$	$(B_{NIR}-B_{BLUE})/(B_{NIR}-B_{GREEN})^2_w$	1/SB	0.22	0.10
SPOT-5	SIPI	$(B_{NIR}-B_{GREEN})/(B_{NIR}-B_{RED})$	SB	0.03	0.54
SPOT-5	NDVI	$(B_{NIR}-B_{RED})/(B_{NIR}+B_{RED})$	SB	0.01	0.79
SPOT-5	$SIPI^2_w$	$(B_{NIR}-B_{GREEN})/(B_{NIR}-B_{RED})^2_w$	SB	0.16	0.17

P: Probability value for the regression model; SIPI: Structure insensitive pigment index; R_{800} and R_{449}: Reflectance values of wavebands centered at 800 and 449 nm of the electromagnetic spectrum; NDVI: Normalized difference vegetation index; MSIPI: Modified SIPI; ETM+: Enhanced Thematic Mapper Plus; SPOT-5: Le System Pour l'Observation de la Terre-5; B_{NIR} and B_{BLUE}: Near infrared and blue bands of ETM+ and SPOT-5, 1/SB: Inversion of SB; $_w$: weighted variable.

Table 5. Coefficients of determination (R^2) associated with vegetation indices and total biomass without sagebrush only green biomass (TBWSB) collected in Yellowstone National Park, Wyoming, United States of America, on August 7-8, 1999.

Instrument	Index	Index Formula	Variable	R^2	P
Probe-1	SIPI	$(R_{800}-R_{449})/(R_{800}-R_{678})$	TBWSB	0.56	< 0.01
Probe-1	NDVI	$(R_{845}-R_{648})/(R_{845}+R_{648})$	TBWSB	0.58	< 0.01
Probe-1	MNDVI	$(R_{1288}-R_{693})/(R_{1288}+R_{693})$	TBWSB	0.91	< 0.01
ETM+	SIPI	$(B_{NIR}-B_{BLUE})/(B_{NIR}-B_{RED})$	TBWSB	0.66	< 0.01
ETM+	NDVI	$(B_{NIR}-B_{RED})/(B_{NIR}+B_{RED})$	TBWSB	0.60	< 0.01
ETM+	$SIPI^2$	$(B_{NIR}-B_{BLUE})/(B_{NIR}-B_{RED})^2$	LogTBWSB	0.80	< 0.01
SPOT-5	SIPI	$(B_{NIR}-B_{GREEN})/(B_{NIR}-B_{RED})$	TBWSB	0.68	< 0.01
SPOT-5	NDVI	$(B_{NIR}-B_{RED})/(B_{NIR}+B_{RED})$	TBWSB	0.59	< 0.01
SPOT-5	$SIPI^2$	$(B_{NIR}-B_{GREEN})/(B_{NIR}-B_{RED})^2$	LogTBWSB	0.78	< 0.01

P: Probability value for the regression model; SIPI: Structure insensitive pigment index; R_{800} and R_{449}: Reflectance values of wavebands centered at 800 and 449 nm of the electromagnetic spectrum; NDVI: Normalized difference vegetation index; MNDVI: Modified NDVI; ETM+: Enhanced Thematic Mapper Plus; SPOT-5: Le System Pour l'Observation de la Terre-5; B_{NIR} and B_{BLUE}: Near infrared and blue bands of ETM+ and SPOT-5, LogTBWSB: Logarithm of TBWSB.

Table 6. Coefficients of Determination (R^2) associated with vegetation indices and woody vegetation index (WVI) collected in Yellowstone National Park, Wyoming, United States of America, on August 7-8, 1999.

Instrument	Index	Index Formula	Variable	R^2	P
Probe-1	SIPI	$(R_{800}-R_{449})/(R_{800}-R_{678})$	WVI	0.05	0.46
Probe-1	NDVI	$(R_{845}-R_{648})/(R_{845}+R_{648})$	WVI	0.05	0.48
Probe-1	MSIPI	$(R_{896}-R_{570})/(R_{896}-R_{601})$	WVI	0.71	0.41
Probe-1	$MSIPI^2$	$(R_{896}-R_{570})/(R_{896}-R_{601})^2$	WVI^2_w	0.96	< 0.01
TM+	NDVI	$(B_{NIR}-B_{BLUE})/(B_{NIR}-B_{RED})$	WVI	0.05	0.46
TM+	SIPI	$(B_{NIR}-B_{RED})/(B_{NIR}+B_{RED})$	WVI	0.07	0.37
TM+	MSIPI	$(B_{NIR}-B_{BLUE})/(B_{NIR}-B_{GREEN})$	WVI	0.26	0.08
TM+	MSIPI	$(B_{NIR}-B_{BLUE})/(B_{NIR}-B_{GREEN})$	$1/WVI_w$	0.73	< 0.01
SPOT-5	SIPI	$(B_{NIR}-B_{GREEN})/(B_{NIR}-B_{RED})$	WVI	0.10	0.30
SPOT-5	NDVI	$(B_{NIR}-B_{RED})/(B_{NIR}+B_{RED})$	WVI	0.05	0.48
SPOT-5	MSIPI	$(B_{MIR}-B_{GREEN})/(B_{MIR}-B_{RED})$	WVI	0.20	0.13
SPOT-5	$MSIPI^2$	$(B_{MIR}-B_{GREEN})/(B_{MIR}-B_{RED})^2$	WVI^2_w	0.29	0.06

P: Probability value for the regression model; SIPI: Structure insensitive pigment index; R_{800} and R_{449}: Reflectance values of wavebands centered at 800 and 449 nm of the electromagnetic spectrum; NDVI: Normalized difference vegetation index; MSIPI: Modified SIPI; ETM+: Enhanced Thematic Mapper Plus; SPOT-5: Le System Pour l'Observation de la Terre-5; B_{NIR} and B_{BLUE}: Near infrared and blue bands of ETM+ and SPOT-5, 1/WVI: Inversion of WVI; $_w$: weighted variable, B_{MIR}: Middle infrared bands of SPOT-5.

remote sensing instruments for TB prediction are presented in Table 3. Non-transformed TB was poorly related (R^2 from 0.32 to 0.33) with the original NDVI $(R_{845}-R_{648})/(R_{845}+R_{648}$: R_{845} and R_{648} refer to reflectance of wavelength centers at 845 and 648 nm) of PROBE-1 and $(B_{NIR}-B_{RED})/(B_{NIR}+B_{RED}$: $B_{NIR}-B_{RED}$ refer to NIR and Blue bands of ETM+ and SPOT-5) of ETM+ and SPOT-5, whereas there were poor to moderate relationships (R^2 from 0.31 to 0.47) between non-transformed TB and original SIPI $(R_{799}-R_{449})/(R_{799}-R_{678})$ of Probe-1, $(B_{NIR}-B_{BLUE})/(B_{NIR}-B_{RED})$ of ETM+, and $(NIR_{NIR}-B_{GREEN})/(B_{NIR}-B_{RED})$ of SPOT-5 (Table 3). P values for the regression models equaled 0.01 or < 0.01 for only SIPI of ETM+ and SPOT-5 (Table 3). This suggested that only these models were statistically significant at $\alpha = 0.01$ to predict TB. The relationships between TB and vegetation indices were improved by using the modified NDVI of Probe-1 (Table 3). The transformed data further improved the relationships between TB and modified vegetation indices. About 83%, 55%, and 84% of the variation in inversion of TB was explained by the square of Probe-1-derived and modified NDVI $(R_{896}-R_{724})/(R_{896}-R_{724})$ of Probe-1, SIPI $(B_{NIR}-B_{BLUE})/(B_{NIR}-B_{RED})$ of ETM+, and $(NIR_{NIR}-B_{GREEN})/(B_{NIR}-B_{RED})$ of SPOT-5, respectively (Table 3). P values for the regression model and indices were < 0.01, implying statistical significance of the regression model to predict TB.

Sagebrush only green biomass (SB)

No statistically significant model was generated at $\alpha = 0.01$ (R^2 ranged from 0.01 to 0.22) between non-transformed SB and original or modified vegetation indices except for the Probe-1-derived SIPI although the relationships were improved by transforming and weighting the data (Table 4). Vegetation indices, procedures applied to the original data, and R^2 and probability (P) values for each of the 3 remote sensing instruments for SB prediction are presented in Table 4. The R^2 value increased from 0.01 to 0.79 using the Probe-1–derived and modified SIPI $(R_{944}-R_{438})/(R_{944}-R_{678})$ for SB estimation (Table 4). This model was statistically significant at $\alpha = 0.01$. Furthermore, a strong and statistically significant relationship at $\alpha = 0.01$ was found between square of Probe-1–derived and modified SIPI and weighted SB ($R^2 = 0.93$).

Total biomass without sagebrush only green biomass

The relationships was good ($R^2 = 0.58$) between NDVI $(R_{845}-R_{648})/(R_{845}+R_{648})$ of Probe-1 and TBWSB. TBWSB exhibited a better relationship with the SIPI $(B_{NIR}-B_{BLUE})/(B_{NIR}-B_{RED})$ of ETM+ ($R^2 = 0.66$), and $(NIR_{NIR}-B_{GREEN})/(B_{NIR}-B_{RED})$ of SPOT-5 ($R^2 = 0.68$) than the NDVI of Probe-1. Table 5 contains information on vegetation indices, procedures applied to the original data, and R^2 and probability (P) values for each of the 3 remote sensing instruments for TBWSB prediction. Modified NDVI $(R_{1288}-R_{693})/(R_{1288}+R_{693})$ derived from Probe-1 had the strongest relationship with TBWSB ($R^2 = 0.91$), whereas the squares of original SIPI $(B_{NIR}-B_{BLUE})/(B_{NIR}-B_{RED})$ of ETM+ and $(B_{NIR}-B_{GREEN})/(B_{NIR}-B_{RED})$ of SPOT-5 had R^2 values of 0.80 and 0.78, respectively, for the logarithmic transformation of TBWSB. The relationships were weaker between original SIPI derived from Probe-1 and TBWSB ($R^2 = 0.56$), between NDVI of ETM+ and TBWSB ($R^2 = 0.60$), and between NDVI of SPOT-5 ($R^2 = 0.59$) when compared with the results obtained from modified NDVI of Probe-1 and transformed data. P values for all models were < 0.01, which indicates that all models generated were statistically significant to estimate TBWSB.

Woody vegetation index

Similar to the SB estimation, a very weak relationship was found between the original or modified vegetation indices and WVI. There was no statistically significant model for WVI prediction (Table 6). However, the relationships between the vegetation indices and WVI were greatly improved using the squares of modified SIPI $(R_{896}-R_{570})/(R_{896}+R_{601})$ of Probe-1 WVI and using the modified SIPI $(B_{NIR}-B_{BLUE})/(B_{NIR}-B_{GREEN})$ of ETM+ and the inversion of WVI. Vegetation indices, procedures applied to the original data, and R^2 and probability (P) values for each of the 3 remote sensing instruments for TB prediction are presented in Table 3. Among the biomass components, the square of SIPI derived from Probe-1 exhibited the highest relationship ($R^2 = 0.96$) with the square of WVI. Modified SIPI of ETM+ exhibited a good and statistically significant relationship ($R^2 = 0.73$, P < 0.01) with inversion of WVI, whereas original or modified SIPI of SPOT-5 had an insignificant relationship at $\alpha = 0.01$ with WVI and its transformations.

The relationships between vegetation indices and biomass components found in this research seem to agree with the findings of some previous studies. Wylie et al. (1996) reported R^2 values ranging from 0.49 to 0.57 for the vegetation indices and grassland live biomass. They stated that live biomass in the shrub covered areas yielded significantly lower relationships with vegetation indices when compared to biomass in grass covered areas. Todd et al. (1998) studied the relationship between vegetation indices derived from a TM-5 scene and biomass in grazed, ungrazed, and combined grazed and ungrazed shortgrass rangelands. They found that vegetation indices were linearly related to biomass collected in the grazed site (R^2 = 0.62-0.67), whereas there was no significant relationship between vegetation indices and biomass obtained from the ungrazed site. Combined biomass from grazed and ungrazed sites was not significantly related to vegetation indices and poorly related to red band (R^2 = 0.35). The authors also reported that correlations between biomass and vegetation indices were improved when biomass of prickly pear cactus (*Opuntia polyacantha*) was removed from the analysis. McGwire et al. (2000) argued that linear mixture modeling analysis could be strongly influenced by the species composition. They found, for example, that inclusion of littleleaf ratany (*Krameria erecta*) in the analysis significantly influenced the R^2 value for total green cover. Standing litter of black grama (*Bouteloua eriopoda*) had different reflectance features than those of other herbaceous species (Asner and Lobell, 2000). Indeed, spectral response of standing litter of black grama was similar to the reflectance of green vegetation in the range from 2100 to 2400 nm of the electromagnetic spectrum. These may indicate that the weak relationships between untransformed biomass components and unmodified vegetation indices might be caused by the presence of a large amount of nonphotosynthetic branch and twig materials interacting directly with incoming light in comparison to the amount of green leaves. Another reason for the weak relationship for the sagebrush component is that some arid-adapted shrubs may be spectrally indeterminate (Okin et al., 2001)

In general, hyperspectral spectral vegetation indices had stronger relationships with the biomass components than the multispectral vegetation indices except for a small difference for TB. A number of authors (Roberts et al., 1993; Vane et al., 1993; Asner, 1998; Thenkabail et al., 2000; Shippert, 2004) have pointed out the superiority of narrowband/hyperspectral imaging spectrometers (e.g., AVIRIS) over broadband/multispectral instruments (e.g., TM) to quantify surface features such as biomass. Narrowband/hyperspectral spectrometers collect spectral information in continuous, narrow spectral channels usually from the 400-2500 nm portion of the spectrum. Multispectral imaging sensors gather spectral data in large, noncontiguous parts of the spectrum; thus a single band represents the average of a relatively large portion of the spectrum. In contrast to broadband remote sensing systems, imaging spectrometers, such as PROBE-1, collect spectral data with an average of 15 nm bandwidth from the 420 to 2500 nm region of the spectrum. Hyperspectral imaging systems have the ability to separate the surface optical properties into many bands, each of which can be investigated individually. However, it is worthwhile to note that the simulated SPOT-5 and ETM+ band derived spectral indices used in this paper may not reflect the real performance of these sensors to record reflected spectra by the vegetation system.

The SIPIs of SPOT-5 and ETM+ have the potential to predict biomass components and these indices accounted for a considerably large proportion of the variation explained in TB and TBWSB. Approximately 84% and 80% of the variation in TB was explained by simulated SPOT-5- and ETM+-derived SIPIs, respectively, while TBWSB accounted for about 80% of the variation for the simulated SIPI of ETM+ and 78% for the simulated SIPI of SPOT-5. However, insignificant relationships were found between SB and the simulated SIPI of SPOT-5 (R^2 = 0.16) and SIPI of ETM+ (R^2 = 0.22). The simulated ETM+-derived SIPI yielded a significant model with a fairly strong relationship (R^2 = 0.73 and $P < 0.01$) for WVI. In contrast to this result, the simulated SPOT-5-derived SIPI had a much weaker and insignificant correlation (R^2 = 0.29) with WVI.

The current research resulted in identifying the most informative regions of the spectrum to estimate biomass components using the possible combinations of NIR and visible band centers in NDV and SIP indices. This suggests that classical wavebands, originally used to developed spectral vegetation indices, could be replaced with others if available. Namely, different band combinations in vegetation indices can be tested using hyperspectral data to reveal the maximum information needed for targeted objects because their spectral properties differ in time and space. Similar findings were observed in earlier

studies. Thenkabail et al. (2000) and Asner and Lobell (2000) argued that the combination of wavebands that provide optimal information to estimate plant biophysical parameters are highly dependent on the current conditions of the target variables. Such things as phenology, plant and soil moisture, chemical contents, and atmospheric conditions are important because reflectance characteristics of soils and plant communities are spatially and temporally dynamic over time. In addition, the use of 12 bands was recommended for optimal crop information retrievals by Thenkabail et al. (2000, 2002) and 22 narrowbands to characterize agricultural crops, shrubs, grasses, and weeds for spectral data collected in African savanna (Thenkabail et al., 2004), which were most likely influenced by the changes in vegetation and soil spectral properties through time and space.

Furthermore, the results of current study indicate that stepwise and weighted regression, and transformation of data can be successfully employed to estimate plant biomass in a big sagebrush region using spectral data with an accurate measurement of surface variables. Information in both imagery pixels and ground plots was not averaged and no outliers were removed from the analyses. Therefore, a minimum experimental error was introduced into the data analysis in this study. It appears that spatial and spectral analyses of a remote sensing imagery can play a major role in the study of vegetation characteristics. This suggests the importance of selecting the appropriate remote sensing instrument for the targeted ecological variables, depending on the scale of the area. Jakubauskas et al. (2001), who studied biophysical parameters of montane sagebrush communities using SPOT XS data, concluded that biophysical characteristics of several sagebrush communities were predictable using spectral data. They further outlined that ecological and phenological properties of vegetation systems to be studied should be considered to select remote sensing instruments for biophysical investigations. The appropriate selection of remote sensing sensors was also highlighted by Jianlong et al. (1998) for studying yield estimation.

Conclusions

In this study we used hyperspectral remote sensing data and simple linear regressions to quantify the relationships between biomass components collected in a big sagebrush dominated area and vegetation indices. The NDVI and SIPI were examined using the all possible band combinations in the visible and infrared portion of the electromagnetic spectrum (423-2507 nm) to estimate biomass components. Findings in this study showed that high spatial and spectral resolution hyperspectral imagery has high potential for biomass estimation by capturing the variability in big sagebrush areas with the establishment of appropriate ground sampling strategy and size. To a lesser degree, simulated, broadband-derived spectral vegetation indices may be able to predict green biomass of vegetation communities dominated by big sagebrush but do not seem to be promising for biomass of homogeneous big sagebrush stands based on the data used in this research. The relationships between biomass components and rich hyperspectral data were improved using different band combinations in traditional vegetation indices and transformed data (Tables 3-6). In addition to simple linear regression, other methods should be considered, such as principle component analysis, discriminant analysis, derivative transformations, modified partial least square, and linear mixture modeling. Additional studies are needed on green and woody sagebrush biomass estimation through the use of hyperspectral and multispectral data to verify the results found in this study.

Acknowledgments

This study was supported by the NASA Earth Observations Commercial Applications Program-Hyperspectral (EOCAP-Hyperspectral); Ministry of National Education, Republic of Turkey; and the National Science Foundation (DEB-9627928) and USDA-NRICGP (93-00501 and 99-00979). We would like to thank the people in these organizations.

References

Asner, G.P. 1998. Biophysical and biochemical sources of variability in canopy reflectance. Remote Sens. Environ. 64: 234-253.

Asner, G.P. and D.B. Lobell. 2000. A biogeophysical approach for automate SWIR unmixing of soils and vegetation. Remote Sens. Environ. 74: 99-112.

Aspinall, R.J., W.A. Marcus and J.W. Boardman. 2002. Considerations in collecting, processing and analyzing high spatial resolution hyperspectral data for environmental investigations. J. Geographical Syst. 4: 15-29.

Barmore, W.J. 1980. Population characteristics, distribution, and habitat relationship of six ungulate species on winter range in Yellowstone National Park. Yellowstone National Park, Final Report Yellowstone files, Mammoth, Wyoming, USA.

Beetle, A.A. and K.L. Johnson. 1982. Sagebrush in Wyoming. Univ. of Wyoming, Agr. Exp. Sta. Bull No. 779. Laramie, Wyoming, USA.

Bork, E.W., N.E. West, K.P. Price and J.W. Walker. 1999. Rangeland cover component quantification using broad (TM) and narrow-band (1.4 NM) spectrometry. J. Range Manage. 52: 249-257.

Earth Search Sciencies, Inc. (ESSI). 2001. http://www.earthsearch.com

Gemmell, F. and J. Varjo. 1999. Utility of reflectance model inversion versus two spectral indices for estimating biophysical characteristics in boreal forest test site. Remote Sens. Environ. 68: 95-111.

Jakubauskas, M., K. Kindscher and D. Debinski. 2001. Spectral and biophysical relationships of montane sagebrush communities in multi-temporal SPOT XS data. Int. J. Remote Sens. 22: 1767-1778

Jianlong, L., L. Tiangang and C. Quangong. 1998. Estimating grassland yields using remote sensing and GIS technologies in Chine. New Zeal. J. Agr. Res. 41: 31-38.

McArthur, E.D. and B.L. Welch. 1982. Growth rate differences among big sagebrush (*Artemisia tridentata*) accessions and subspecies. J. Range Manage. 35: 396-401.

McGwire, K., T. Minor and L. Fenstermaker. 2000. Hyperspectral mixture modeling for quantifying sparse vegetation cover in arid environments. Remote Sens. Environ. 72: 360-374.

Okin, G.S., D.A. Roberts, B. Murray and W.J. Okin. 2001. Practical limits on hyperspectral vegetation discrimination in arid and semiarid environments. Remote Sens. Environ. 77: 360-374.

Peñuelas, J., F. Baret and I. Filella. 1995. Semi-empirical indices to assess carotenoids/chlorophyll *a* ratio from leaf spectral reflectance. Photosynthetica. 31: 221-230.

Ramsey, R.D., D.L. Wright and C. McGinty. 2004. Evaluation the use of 30m Enhanced Thematic Mapper to monitor vegetation cover in shrub-steppe environments. Geocarto International 19: 39-47.

Roberts, D.A., M.O. Smith and J.B. Adams. 1993. Green vegetation, nonphotosynthetic vegetation, and soils in AVIRIS data. Remote Sens. Environ. 44: 255-269.

Rouse, J.W., R.H. Naas, J.A. Schell and D.W. Deering. 1973. Monitoring vegetation systems in the Great Plains with ERTS, pp. 309-317. *In*: Third ERST Symposium, NASA Sp-351, Vol. 1, Washington, DC, USA.

Shippert, P. 2004. Why use hyperspectral imagery? Photoramm. Eng. Rem. S. 70: 377-380.

Simon, S. 2006. Log transformation. Available online at: http://www.childrens-mercy.org/stats/model/linear/log.asp

S-PLUS. 2001. S-PLUS 6 for Windows guide to statistics. Vol. 1. Insightful Inc, Seattle, WA.

Thenkabail, P.S., R.B. Smith and E. De Pauw. 2000. Hyperspectral vegetation indices and their relationships with agricultural crop characteristics. Remote Sens. Environ. 71: 158-182.

Thenkabail, P.S., R.B. Smith and E. De Pauw. 2002. Evaluation of narrowband and broadband vegetation indices for determining optimal hyperspectral wavebands for agricultural crop characterization. Photogramm. Eng. and Rem. S. 68: 607-621.

Thenkabail, P.S., E.A. Enclona, M.S. Ashton and B. Van Der Meer. 2004. Accuracy assessments of hyperspectral waveband performance for vegetation analysis applications. Remote Sens. Environ. 91: 354-376.

Todd, S.W., R.M. Hoffer and D.G. Milchunas. 1998. Biomass estimation on grazed and ungrazed rangelands using spectral indices. Int. J. Remote Sensing 19: 427-438.

Vane, G., R.O. Green, T.G. Chrien, H.T. Enmark, E.G. Hansen and W.M. Porter. 1993. The airborne visible/infrared imaging spectrometer (AVIRIS). Remote Sens. Environ. 44: 127-143.

Wylie, B.K., D.D. DeJong, L.L. Tieszen and M.E. Biondini. 1996. Grassland canopy parameters and their relationships to remotely sensed vegetation indices in the Nebraska Sand Hills. Geocarto International 11: 39-51.